Fault Ride-Through for Hydrogen Electrolyzers

Mohammadhossein Tavanaee, Marc Cheah-Mañe, Oriol Gomis-Bellmunt, and Eduardo Prieto-Araujo
CITCEA-UPC, Universitat Politècnica de Catalunya (UPC), Barcelona, Spain
Emails: {mohammadhossein.tavanaee, marc.cheah, oriol.gomis, eduardo.prieto-araujo}@upc.edu

***Abstract*—This paper investigates the Fault Ride-Through (FRT) capability of a Proton Exchange Membrane (PEM) electrolyzer system supported by Supercapacitor (SC) energy storage under symmetrical fault conditions. Three configurations are analyzed: a baseline case without SC integration, SCs directly connected to the DC link, and SCs interfaced via a DC/DC converter. To evaluate the system behavior under these configurations, a dynamic model of the PEM electrolyzer is implemented to capture its transient response. Based on this model, analytical formulas are derived for sizing the energy buffer required to maintain continuous operation during grid disturbances. In parallel, a unified control strategy is proposed to coordinate power flow between the grid, SCs, and the electrolyzer. Time-domain simulations confirm that only the SC-supported configurations maintain uninterrupted hydrogen production during a severe grid voltage sag. The DC/DC-based layout reduces the number of SCs and offers greater control flexibility, while the direct connection provides a simpler solution. These results provide design insight for the robust integration of hydrogen systems into future power grids.**

I. Introduction

Green hydrogen produced by water electrolysis driven solely by renewable electricity is widely regarded as a pivotal technology for decarbonizing Europe's power and industrial sectors [1]. Under the European Green Deal, the EU has committed to reducing greenhouse gas emissions by at least 55% by 2035 and achieving climate neutrality by 2050 [2]. To achieve these targets, large-scale electrolyzer plants must be reliably integrated into the grid. This integration necessitates compliance with specific grid codes; for instance, The European Network of Transmission System Operators for Electricity (ENTSOE) advises grid operators to incorporate Fault Ride-Through (FRT) capabilities, defined as the ability to remain connected and provide support during voltage sags, into their hydrogen systems [3]. Similarly, the updated German grid code mandates converter manufacturers to implement these capabilities as well [4]. Unlike wind or PV systems, where DC-link voltage rises during faults, electrolyzer systems experience a voltage collapse, requiring energy storage rather than dissipation to maintain operation.

While extensive research has addressed FRT capabilities for inverter-based renewables such as wind and PV systems, relatively fewer studies have focused on FRT for electrolyzers. Additionally, the impact of power fluctuations on Proton Exchange Membrane (PEM) electrolyzers is not yet thoroughly understood, though several studies highlight potential risks. For example, current ripple at low frequencies has been shown to accelerate the degradation of the Membrane Electrode Assembly (MEA), reducing system efficiency and durability [5], [6]. Dynamic operation, characterized by intermittent power supply typical of renewable sources, also contributes to increased resistance and reversible degradation in PEM electrolyzers [7], emphasizing the need for energy storage to protect these systems.

SCs are especially well-suited for FRT applications due to their exceptional power density, fast response time, and long cycle life [8]. Compared to other technologies such as batteries, flywheels, or conventional capacitors, they offer faster energy delivery with minimal maintenance and high efficiency, making them ideal for managing short-duration, high-power disturbances [9]. Their compact size and scalability further enhance their suitability for grid-connected hydrogen systems.

In this paper, the FRT performance of a PEM electrolyzer interface via a Voltage Source Converter (VSC) that is supported by an SC storage is analyzed. The study begins with the analytical derivation of the minimum energy buffer required during grid faults, followed by the development of a unified control architecture for the VSC and both DC/DC converters. Finally, time-domain simulations are carried out to validate the FRT capability under symmetrical fault conditions.

To the best of the authors' knowledge, no prior study has combined uninterrupted hydrogen production during three-phase faults via a compact SC sizing method linked to DC-link and converter limits, a comparison of direct versus DC/DC SC integration with quantified design trade-offs, and benchmarking against a no-storage baseline to demonstrate the need for buffering under fault conditions.

The study results demonstrate that an appropriately sized SC configuration can maintain continuous hydrogen output during grid disturbances, thereby offering a practicable route to satisfy forthcoming grid-code FRT mandates with minimal additional storage investment.

II. System Description

The overall system architecture considered in this study is shown in Fig. 1. VSC technology is selected for AC/DC conversion due to its controllability and dynamic performance under grid disturbances. The VSC operates as a rectifier and interfaces the Medium Voltage (MV) grid to the DC link through a step-down transformer.

A DC/DC converter connects the PEM electrolyzer to the DC link, allowing voltage regulation and reducing current stress on the VSC switches. To ensure uninterrupted electrolyzer operation during grid faults, an energy storage system based on SCs is integrated on the DC side. The SCs can be connected either directly to the DC link or via a DC/DC converter, depending on the configuration under study.

A three-phase symmetrical fault is applied at the Point Of Connection (POC) between the VSC and the MV grid. The system response to this disturbance is analyzed in subsequent sections.

979-8-3315-2503-3/25/$31.00 ©2025 IEEE

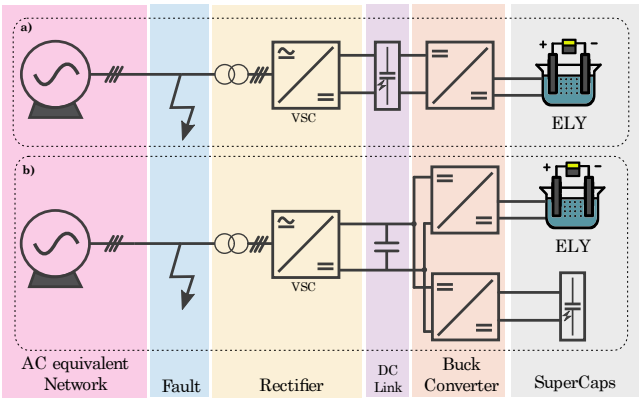

Fig. 1: System description

III. Energy Storage Calculation

To maintain continuous hydrogen production during grid disturbances, an energy buffer must compensate for the temporary power loss from the grid. In this study, an SC module is integrated into the DC side of the system to support the electrolyzer during symmetrical fault events.

The minimum required capacitance for the SC bank is estimated by:

$$C = \frac{2S_N \tau_C}{V_{dc(max)}^2 - V_{dc(min)}^2}, \tag{1}$$

Where S_N is the nominal power of the converter, τ_C is the target support duration, and $V_{dc(max)}$, $V_{dc(min)}$ represent the acceptable voltage range across the DC link during the fault, in this study for instance, the $V_{dc(max)}$ is equal to the nominal DC voltage and $V_{dc(min)}$ is considered as 60%. However, these thresholds can be adjusted based on the specific capabilities of the converter.

This formulation assumes that the SC delivers the full power required by the electrolyzer during the fault, ensuring that the DC link voltage remains within safe operational limits. Additional considerations, such as the internal resistance, peak current, and rated voltage of the SC units, are addressed in the design and sizing process in the following sections.

IV. Energy storage modelling

The Rint-Capacity model is a widely used model for SCs and comprises a capacitor and a resistor. The charge that instantly accumulates on the SC electrode's surface is signified with C_0. The internal resistance provided by the separator, the electrode pores, the contact resistance between the electrodes and current collectors, and the electrolyte are represented with a lumped resistance R_{esr} [10]. The full model is represented with the following equation:

$$V_t = \frac{1}{C_0}\int I\,dt - R_{\text{esr}} I, \tag{2}$$

In power electronic applications, this model's simplicity and sufficient precision make it suitable to be used for modeling purposes.

V. Energy storage design

There are two methods considered to design the layout of the energy buffer in the DC link: either SCs are connected directly to the DC link or SCs are connected to the DC link via a DC/DC converter. In order to take into account a practical implementation for the energy storage design, SC manufacturer datasheets are considered in this study. The names of the SC manufacturers are omitted to prevent potential commercial bias in the comparative analysis. The relevant specifications are provided in Table I.

TABLE I: Supercapacitors specifications

Parameters	***Manfacturer 1***	***Manfacturer 2***	***Manfacturer 3***	***Manfacturer 4***	***Manfacturer 5***
Capacitance (F)	3000	3400	3000	3400	3000
Voltage (V)	2.7	3	2.5	2.85	3
Max Continuous Current (A)	170-280	160-270	140-230	143	143
Max Peak Current (A)	2300	2800	2165.78	2700	2400
Internal Resistance ESR (mΩ)	0.15-0.23	0.13-0.23	0.29	0.23	0.23
Stored Energy (Wh)	3.0	4.2	3.0	3.8	3.8
Volume (m3)	3.95e-4	3.95e-4	3.95e-4	3.95e-4	3.95e-4

Primarily, the energy requirement during the fault must be calculated to obtain the needed capacitance. Equation (1) can be applied subsequently to determine the minimum capacitance required to withstand the fault. The next crucial step is to obtain the required number of series and parallel capacitors by taking into account the data in the Table I, which can be calculated as

$$N_s = \frac{V_{DC}}{V_{SC}}, \quad N_p = \frac{I_{DC}}{I_{SC_{\text{peak}}}} \tag{3}$$

where N_s is the number of cells in series, V_{DC} is the DC link nominal voltage and V_{SC} is the SC cell voltage.
N_p is the number of modules in parallel, I_{DC} is the DC link nominal current, and $I_{SC_{peak}}$ is the peak current that each SC can provide for a maximum of 1 second until its voltage drops by 50% [11]. Since the aim of implementing this energy storage in this study is to provide power during faults, which are often in the millisecond range, the peak or pulse current of SCs can be addressed in the design.

A. Configuration without DC/DC converter

Omitting a DC/DC converter simplifies the system architecture and reduces cost by eliminating the need for an additional power stage. However, given the high DC link voltage, a large number of SC cells must be connected in series to meet the voltage requirement. This configuration increases the total Equivalent Series Resistance (ESR), which negatively impacts performance during transient events. In fault conditions where fast energy delivery is critical, higher internal resistance leads to greater losses and reduced effectiveness in maintaining the DC link voltage. The sizing and performance results for this direct connection layout are summarized in Table II.

B. Configuration with DC/DC Converter

Integrating SCs via a dedicated DC/DC converter introduces additional system complexity and cost. However, it

TABLE II: SCs layout without DC/DC converter

Parameters	*Manfacturer 1*	*Manfacturer 2*	*Manfacturer 3*	*Manfacturer 4*	*Manfacturer 5*
DC Voltage (V)	800	800	800	800	800
Series Cells Ns	297	267	320	281	267
Parallel Modules Np	1	1	1	1	1
Total SCs Nsc	297	267	320	281	267
Total Capacity (F)	10.1	12.7	9.3	11.8	11.2
Total Internal Resistance (mΩ)	44.5-68.3	34.7-61.4	92.8	64.6	61.4
Total Stored Energy (Wh)	891	1121.4	960	1067.8	1014.6

TABLE III: SCs with DC/DC converter

Parameters	*Manfacturer 1*	*Manfacturer 2*	*Manfacturer 3*	*Manfacturer 4*	*Manfacturer 5*
DC Voltage (V)	400	330	420	340	380
Series Cells Ns	149	110	168	120	127
Parallel Modules Np	1	1	1	1	1
Total SCs Nsc	149	110	168	120	127
Total Capacity (F)	20.13	30.90	17.85	28.33	23.62
Total Internal Resistance (mΩ)	22.35-34.27	16.5-25.3	48.72	27.6	29.2
Total Stored Energy (Wh)	447	462	508	456	482.6

significantly reduces the number of SC cells required by decoupling the SC voltage from the high DC link voltage. This configuration also enables greater control flexibility, such as facilitating the implementation of Grid-Forming (GFOR) control strategies on the rectifier side.

To determine the optimal operating voltage for the SCs of the DC/DC converter, a parametric sweep was performed based on the electrical specifications of each SC listed in Table I. The analysis evaluates the total number of required SC cells across a range of operating voltages (10–1200 V), using discrete steps of 10 V. The resulting trade-off between voltage level and total capacitor count is shown in Fig. 2, which highlights the voltage range that minimizes component count while avoiding excessive converter losses and current stress.

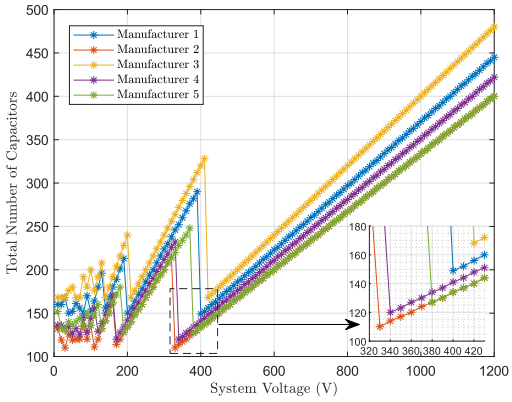

Fig. 2: Number of SCs vs DC voltage

The number of SCs is most favorable at certain voltage levels, as shown in the Fig. 2, between 10 and 200 V. The problem arises from excessive current at too-low voltages and DC/DC converter losses at low-duty cycle ratios [12]. Therefore, depending on each SC standard, the DC voltage levels should be between 330 and 420 V to minimize the number of SCs as well as overcome the mentioned issue. The results are gathered in Table III.

VI. Control Design

The control structure must ensure stable operation and coordinated power flow among the SC, Electrolyzer (ELY), and VSC under normal conditions and be resilient against disturbances. An overview of the full control strategy is illustrated in Fig. 3, comprising three main layers: AC/DC converter control of the VSC, DC/DC converter control for the ELY, and DC/DC converter control for the SC.

The VSC operates in Grid-Following (GFL) mode, where synchronization with the grid is achieved via a Phase-Locked Loop (PLL). Its outer control loops regulate the DC link voltage V_{dc} and reactive power Q, with a voltage droop mechanism incorporated to support the voltage at the POC, following the structure in [13]. To comply with grid code requirements during voltage sags, a current saturation strategy is implemented to prioritize reactive current injection and limit overcurrent conditions.

The ELY's DC/DC buck converter is controlled to track a power reference P^*_{ELY} derived from system-level requirements. A cascaded controller regulates the output current to maintain stable hydrogen production. This structure enables flexible operation even under voltage variations at the DC link [12].

The SC's DC/DC converter control objective is to support the DC link voltage through the energy stored in the storage unit. It operates in a fast-response mode, discharging when V_{dc} drops below its reference and recharging when conditions stabilize. The control prioritizes speed and simplicity to ensure responsiveness under grid disturbances [10].

VII. PEM Electrolyzer Modeling

To model the electrolyzer according to different objectives, several modeling approaches exist. For power system and electrical studies, empirical electrical equivalent models are often employed. For instance, in [14], both static and dynamic electrical models were developed and validated against experimental data from a real PEM electrolyzer. The dynamic model showed significantly higher accuracy, with a maximum error of 4%, compared to 15% for the static model, particularly during current step changes. Based on the modeling approaches presented in [14], [15], the electrical dynamic equivalent model of the PEM electrolyzer used in this study is developed and illustrated in Fig. 4. The voltage at the anode represents the reversible voltage V_{rev}, or Nernst voltage, when the voltage at the electrolyzer terminal surpasses it, causing current to flow. R_{mem} indicates the ohmic losses, which are largely linked to the membrane. The RC branch on the cathode side reflects the activation overpotential, which is responsible for the electrolyzer's first-order voltage response to current variations. While this model captures key electrical dynamics relevant for grid integration studies, it does not account for long-term degradation or aging effects, which would require more detailed physicochemical modeling.

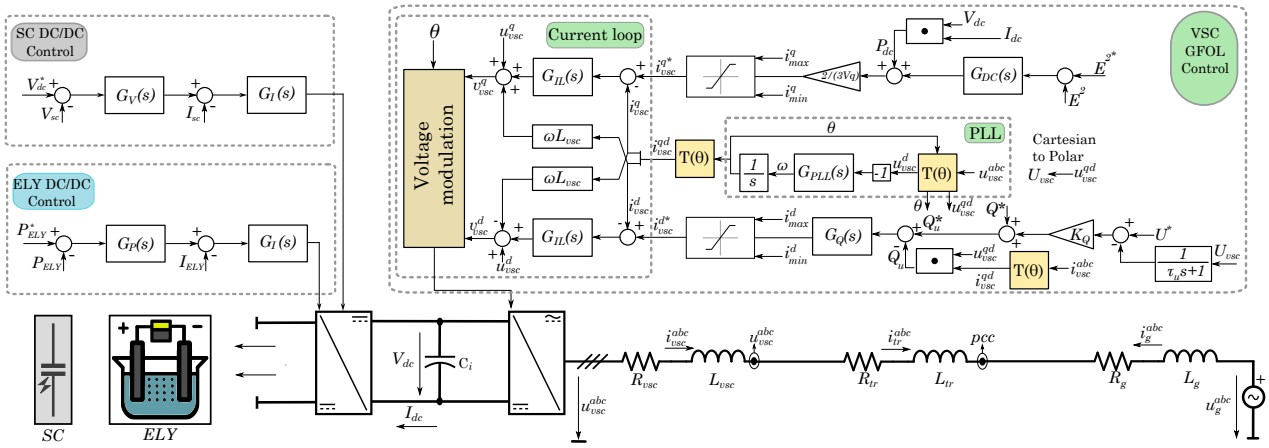

Fig. 3: Overall control scheme

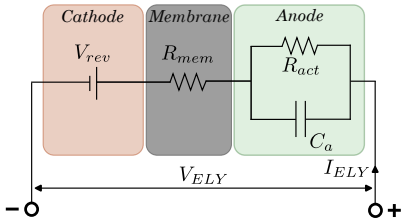

Fig. 4: PEM electrolyzer electrical dynamic equivalent

VIII. Results and Discussion

Time-domain simulations were performed to evaluate the FRT capability of the PEM electrolyzer system under three configurations: a baseline case without any SC integration, included to highlight the impact of energy storage; (a) SCs directly connected to the DC link; and (b) SCs interfaced via a DC/DC converter. All cases are subjected to a symmetrical grid fault in which the voltage at the POC drops to 0.2 pu for 250 ms, starting at 2 s. The system parameters, which also serve as the base quantities for per-unit (pu) normalization, are summarized in Table IV, and the resulting system responses are presented in Fig. 5 and Fig. 6.

TABLE IV: System parameters

Parameter	Unit	Value
AC/DC Converter Nominal Power	MVA	1
Network Voltage	kV	20
Nominal AC Voltage	V	400
Nominal DC Link Voltage	V	800
DC/DC Converter Nominal Power	MW	1
ELY Nominal Power	MW	0.9
ELY Nominal Voltage	V	400

Prior to the fault, the system operates under steady-state conditions, with the electrolyzer receiving approximately 0.9 pu of its nominal power. At 2 s, the fault is initiated, causing V_{rms} to drop to 0.2 pu and I_{rms} to rise to 1 pu until saturation is triggered. Brief current oscillations are observed, but they last only 2–3 ms and do not affect semiconductor reliability.

In the baseline case without SCs, the fault detection logic triggers an immediate interruption of power delivery to the electrolyzer in order to prevent a significant collapse of the DC link voltage. As a result, P_{dc} drops to zero during the fault, leaving the electrolyzer inactive. Although the small DC-link capacitor prevents a complete voltage collapse and enables quick post-fault recovery, the sudden loss of power triggered by the protection system poses a potential risk to the electrolyzer's long-term reliability and continuity of operation. This case clearly illustrates the necessity of energy storage for ensuring stable and uninterrupted hydrogen production during grid disturbances.

Unlike the baseline case, in cases (a) and (b), the fault detection mechanism that disables electrolyzer operation is not required. The SCs provide sufficient energy to support the DC link voltage V_{dc}. Right after fault occurrence, P_{ac} drops to zero due to activation of the saturation logic, while Q_{ac} reaches its limit, injecting approximately 0.2 pu of reactive power to support the grid.

On the DC side, the DC link voltage V_{dc} drop varies depending on the SC characteristics; configurations with less stored energy exhibit more pronounced voltage sag. However, all SC configurations successfully maintain the DC link voltage above the minimum design threshold of 0.6 pu throughout the fault, as established in Section III. Despite the voltage drop, P_{dc} remains stable in both SC-supported scenarios, confirming that the energy buffer effectively decouples the electrolyzer from grid-side disturbances.

Once the fault is cleared at 2.25 s, the current saturation logic is deactivated, and the converter resumes normal operation. As a result, both P_{ac} and Q_{ac} gradually return to pre-fault values. In both SC-supported configurations, P_{ac} temporarily exceeds its pre-fault value due to the combined effect of SC recharging and ongoing electrolyzer supply. This elevated power demand lasts until approximately 5 s, by which time the DC link voltage is fully restored and the system returns to steady-state operation.

Overall, the baseline case, which excludes SC integration, demonstrates the necessity of energy storage to ensure uninterrupted operation and protect the longevity of the electrolyzer during grid disturbances. Simulation results for case (a), where SCs are directly connected to the DC link, and case (b), where SCs are interfaced via a DC/DC converter, confirm that

both configurations effectively maintain FRT capability and preserve continuous hydrogen production. While the DC/DC-based layout (case b) requires fewer supercapacitors, it exhibits a slightly deeper V_{dc} drop due to reduced total stored energy. Nonetheless, both configurations meet the performance objectives under the defined fault conditions.

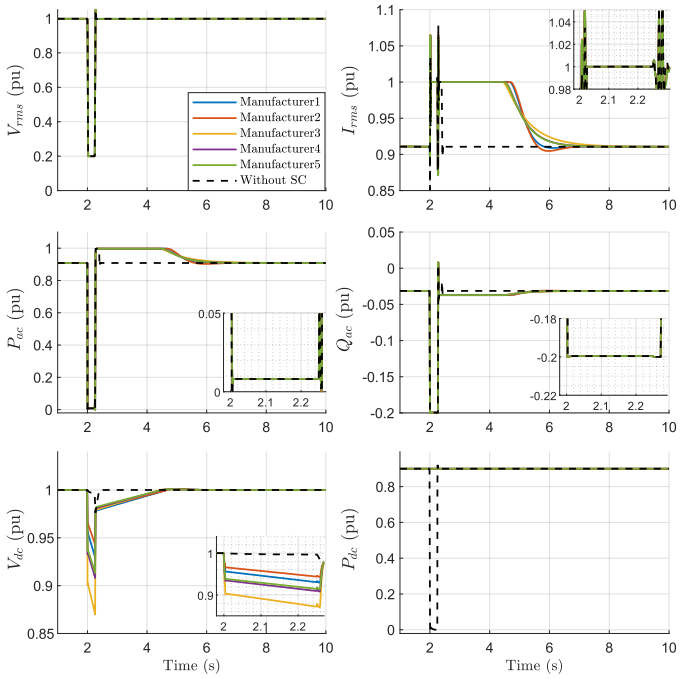

Fig. 5: System response under symmetrical fault, SCs directly connected to DC link (Case a), in addition to baseline case (without SC)

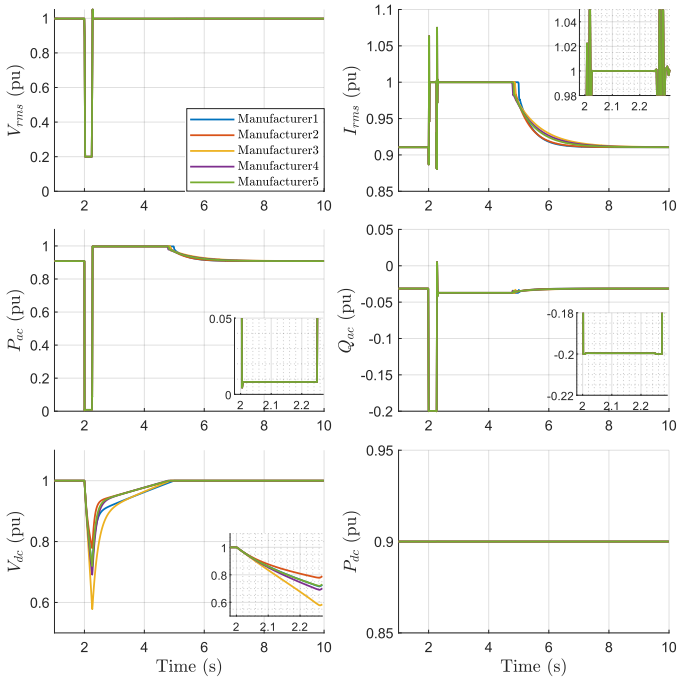

Fig. 6: System response under symmetrical fault, SCs with DC/DC connected to DC link (Case b)

IX. Conclusion

This paper presented a fault ride-through assessment of a PEM electrolyzer system supported by SCs under two connection configurations: direct DC link connection and DC/DC converter integration. Simulation results confirm that both configurations successfully maintain continuous hydrogen production during symmetrical grid faults. The DC/DC-connected layout offers reduced SC count and enhanced modularity, but introduces additional cost and complexity. In contrast, the direct connection is simpler and more economical but requires a larger number of SCs and may compromise electrolyzer operation under non-fault conditions in the event of energy storage failure. These findings highlight the trade-offs between robustness, cost, and design complexity when selecting an energy storage integration strategy for grid-connected hydrogen systems. Future work will focus on experimental characterization of PEM electrolyzers under power oscillations to quantify stack/cell degradation and validate the dynamic model. These data will enable aging-aware SC sizing and control, yielding more accurate and economically optimal designs. Further extensions include validation under unbalanced faults and hardware-in-the-loop testing of the full control stack.

X. Acknowledgment

This work received funding from the European Union's Horizon Europe research and innovation program under the Grant Agreement No. 101092153. Views and opinions expressed are however those of the authors only and do not necessarily reflect those of the European Union or European Health and Digital Executive Agency. Neither the European Union nor the granting authority can be held responsible for them.

References

[1] Kane *et al.*, "Green hydrogen: A key investment for the energy transition," 2022.
[2] European Commission, "2050 long-term strategy," 2023.
[3] ENTSO-E and F. E. Ltd, "European network of transmission system operators for electricity potential of p2h technologies to provide system services," 06 2022.
[4] Netztransparenz.de, "Technische anforderungen für den anschluss von elektrolyseanlagen," 2024.
[5] Parache *et al.*, "Impact of power converter current ripple on the degradation of pem electrolyzer performances," *Membranes*, vol. 12, no. 2.
[6] G. Papakonstantinou *et al.*, "Degradation study of a proton exchange membrane water electrolyzer under dynamic operation conditions," *Applied Energy*, vol. 280, p. 115911, 2020.
[7] Endrődi *et al.*, "Challenges and opportunities of the dynamic operation of pem water electrolyzers," *Energies*, vol. 18, no. 9, 2025.
[8] Durvasulu *et al.*, "Technology strategy assessment: Findings from storage innovations 2030 supercapacitors," Idaho National Laboratory (INL), Idaho Falls, ID (United States), Tech. Rep., 07 2023.
[9] Khodaparastan *et al.*, "Flywheel vs. supercapacitor as wayside energy storage for electric rail transit systems," *Inventions*, vol. 4, no. 4, 2019.
[10] Bansal *et al.*, "Effect of supercapacitor modelling and unit cell capacitance selection towards economic sizing of energy storage system in electric vehicle," *Journal of Energy Storage*, vol. 51, p. 104517, 07.
[11] EATON, "Xvm-315 supercapacitor pcba module," 2019.
[12] N. Mohan, *Power electronics*. Wiley, 2012.
[13] A. Egea-Alvarez *et al.*, *Active and Reactive Power Control of Grid Connected Distributed Generation Systems*, 2012, pp. 47–81.
[14] D. Guilbert and G. Vitale, "Dynamic emulation of a PEM electrolyzer by time constant based exponential model," *Energies*, vol. 12, p. 750, 02 2019.
[15] Yodwong *et al.*, "Proton exchange membrane electrolyzer modeling for power electronics control: A short review," *C*, vol. 6, p. 29, 06 2020.